

# DESIGN ORIENTED ANALYSIS OF A HIGH POWER FACTOR AND LOW COST THREE-PHASE RECTIFIER

**Ewaldo L. M. Mehl<sup>1</sup>**, *Student Member IEEE*

Federal University of Paraná  
Department of Electrical Engineering  
Caixa Postal 19011  
Curitiba, Paraná, 81531-970 BRAZIL  
E-Mail: e.mehl@icece.org

and

**Ivo Barbi**, *Senior Member IEEE*

Federal University of Santa Catarina  
Institute of Power Electronics  
Caixa Postal 5119  
Florianópolis, Santa Catarina, 88040-970 BRAZIL  
E-Mail: ivo@inep.ufsc.br

**Abstract** - The analysis of a new three-phase rectifier with high power factor is presented in this paper, in view of a complete design procedure. The main features of the proposed circuit are low cost, small size, high efficiency and simplicity. With the introduction of the "critical inductance" of the converter, the circuit can be analyzed by a simplified equivalent circuit. A set of linear equations was derived, modeling the input current of the rectifier and demonstrating the high power factor and low harmonic distortion characteristics of the circuit. The theoretical analysis was validated with simulation and experimental results obtained from two laboratory prototypes rated at 7 kW and 12 kW, connected to the 220 V, 60 Hz AC system.

## NOMENCLATURE

$I_{sw(max)}$	maximum current through an active switch
$V_{sw(max)}$	maximum voltage across an active switch
$P_o$	DC output power of the converter
$\psi$	power ratio of the active switch(es)
$V_i$	rms phase-to-phase input voltage
$V_o$	DC output voltage of the converter
$L$	critical inductance
$f$	frequency of the AC source
$\omega$	angular frequency

## I. INTRODUCTION

In the recent years a number of circuits have been proposed to improve the power factor of AC to DC power converters. Prasad, Ziogas and Manias [1] introduced the circuit shown in Fig. 1, where the power factor correction of a three-phase rectifier is achieved with a boost topology with three input inductors. Although that circuit draws a high quality input current from the AC source with near unity power factor, in high power applications the boost active switch stands as a challenging design problem. The "power ratio of the active switch" on that converter can be calculated with Eq. (1):

$$\psi = \frac{I_{sw(max)} \cdot V_{sw(max)}}{P_o} \quad (1)$$

<sup>1</sup> This work was performed at the Power Electronics Institute of the Federal University of Santa Catarina, while E. L. M. Mehl was a student at the Doctorate Program of Electrical Engineering, with financial support from the Brazilian Ministry of Education, under the CAPES/PICD program.

Using the set of design equations found in [1], Eq. (1) gives  $\psi = 4.7$ , showing that a high VA rating is required for the boost switch to perform the power factor correction.

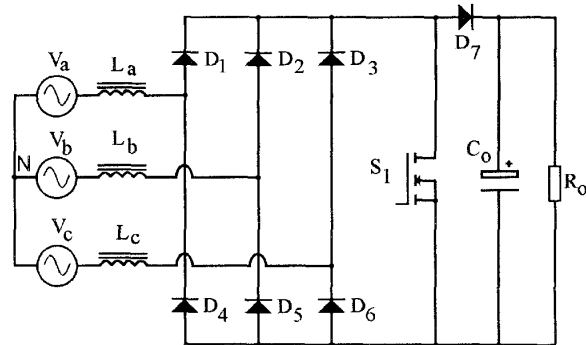


Figure 1: Three-Phase AC to DC converter with a boost power factor correction switch, from Prasad, Ziogas & Manias [1].

In order to overcome the drawbacks from the circuit presented in [1], a new AC to DC converter shown in Fig. 2 was presented in [2] and achieves low harmonic distortion of the input current and high power factor with three low-frequency bi-directional switches ( $S_a$ ,  $S_b$  and  $S_c$ ). On the proposed converter the VA rating of the switches is very low in contrast to the high output power of the converter. As a result, the new circuit accomplishes a "power ratio of the active switches" of  $\psi = 0.907$ . That number shows that the power factor correction can be obtained with low power switches in the new circuit.

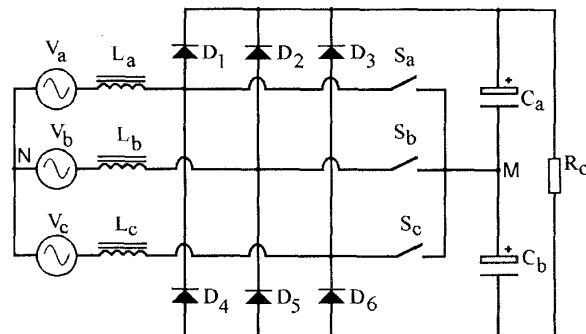


Figure 2: The new three-phase AC to DC converter presented in [2] by Mehl & Barbi.

This paper presents the analysis of the new AC-DC converter presented in [2], in view of a complete design procedure. To validate the theoretical analysis, two laboratory prototypes were built and evaluated by bench tests.

## II. CIRCUIT DESCRIPTION AND ANALYSIS

The circuit originates from a conventional three-phase diode rectifier with input inductors (Fig. 2), completed by three bi-directional low-power switches ( $S_a$ ,  $S_b$ ,  $S_c$ ) connecting the corresponding input inductor with a common central node ( $M$ ) between two high-capacitance filter capacitors ( $C_a$ ,  $C_b$ ). For the present analysis, each switch is gated on when the respective phase voltage is null, with gate pulse width equivalent to  $1/12$  of the voltage period (or  $30^\circ$ ). The power circuit is similar to the high-frequency PWM rectifier presented in [3], but in the proposed circuit the switches operate at line frequency.

Assuming the ACB phase sequence and  $0^\circ$  when the phase voltage  $V_a$  initiates a positive semi-cycle, Fig. 3 shows the gate pulses ( $V_{ga}$ ,  $V_{gb}$ ,  $V_{gc}$ ) of the bi-directional switches  $S_a$ ,  $S_b$  and  $S_c$ . Using suchlike switching pattern, the bi-directional switches operate at low frequency, with reduced power losses and there is no necessity of fast switching semiconductor devices on the proposed circuit. Along with this feature, the input inductors can be assembled with ordinary core materials, resulting in a low cost AC to DC converter with high power factor, suitable to high power applications.

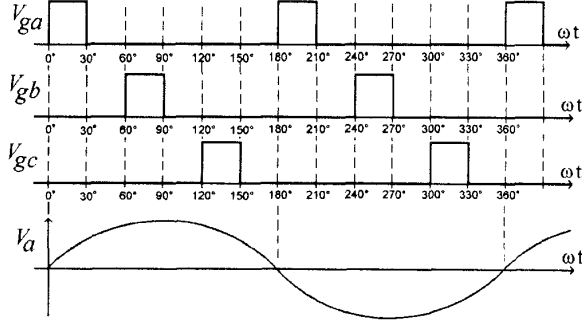


Figure 3: The low-frequency switching pattern presented in [2].

Figure 4 shows the six topological stages of the proposed rectifier for a half period of the input voltage  $V_a$ . For simplicity, in Fig. 4 it is shown only the components under current, at each stage. Supposing ideal diodes, switches with null "on" resistance, and constant DC output voltage, each of the figured stages can be analyzed as a linear circuit. It is also possible to notice two main situations: in (a), (c) and (e) there are two conducting diodes and one switch is gated on; in (b), (d) and (f) there are three conducting diodes and all switches are off. For the stages (a), (c) and (e) the current through the "on" switch is ruled by Eq. (2):

$$i_{sw}(t) = \frac{V_i \cdot \sqrt{2}}{\sqrt{3} \cdot \omega \cdot L} [1 - \cos(\omega \cdot t)] \quad (2)$$

On the other hand, for each stage (b), (d) and (f), the circuit analysis produces differential equations similar to Eq. (3):

$$\frac{d}{dt} i_a(t - t_o) = \frac{V_a(t - t_o)}{L} - \frac{V_o}{3 \cdot L} \quad (3)$$

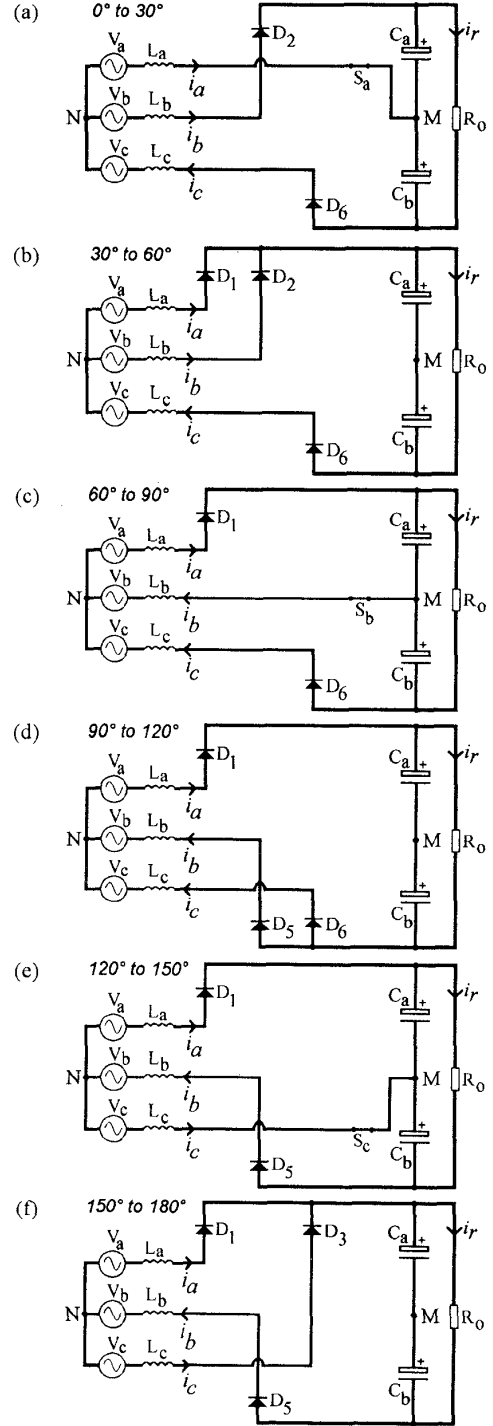


Figure 4: Topological stages for a half-period of the  $V_a$  input voltage.

The differential equations can be solved using Laplace transformation and employing the value of the input current at the end of each stage as the initial value on the next stage. This procedure leads to a set of equations describing the input current as a function of the DC output voltage ( $V_o$ ). For instance, during the  $150^\circ - 180^\circ$  interval the input current on phase A is ruled by Eq. (4):

$$i_a(t) = \frac{\sqrt{2} \cdot V_i}{3 \cdot \omega \cdot L} \left[ \sqrt{3} \sin(\omega \cdot t) + 3 \cos(\omega \cdot t) - 3 \right] + \frac{-V_o}{3 \cdot L} + \frac{3\sqrt{2} \cdot V_i + 2\sqrt{3}\sqrt{2} \cdot V_i - 2\pi \cdot V_o}{6 \cdot \omega \cdot L} \quad (4)$$

On a first approach the system of equations seems to be undetermined. However, there is a particular value to the inductance of the input inductors  $L_a$ ,  $L_b$  and  $L_c$  that can be considered as the "critical inductance" ( $L$ ) of the circuit. With such value of inductance, at  $180^\circ$  and  $360^\circ$  the input current reaches zero, concomitant with the respective phase voltage zero-volt transition. Assuming that Eq. (4) is null for  $\omega \cdot t = 180^\circ$ , the DC output voltage of the converter is obtained as Eq. (5):

$$V_o = \left( \frac{36 \cdot \sqrt{2}}{7 \cdot \pi \cdot \sqrt{3}} \right) \cdot V_i = 13366 \cdot V_i \quad (5)$$

The "critical inductance" can be calculated with Eq. (6), assuming that the input current feeds the load during the  $90^\circ - 120^\circ$  interval of Fig. 4:

$$L = \frac{36}{7} (2\sqrt{3} - 3) \cdot \frac{(V_i)^2}{2 \cdot \pi^3 \cdot f \cdot P_o} = 38489 \times 10^{-2} \cdot \frac{(V_i)^2}{f \cdot P_o} \quad (6)$$

From there on, a simplified equivalent circuit can be derived, shown in Fig. 5. The voltage of the central node M, using the node N as the reference, can be modeled by a three-level pulsed voltage source  $V_p$  as represented in Fig. 6.

The input current on each phase of the three-phase rectifier is described by the set of linear equations seen in Table 1. For the  $180^\circ - 360^\circ$  interval, the same equations can be used, multiplied by (-1). Those equations can be easily programmed on a computer to plot the input current of a generalized converter, as seen in Fig. 7. The vertical axis values on Fig. 7 should be multiplied by the  $\left( \frac{\sqrt{2} \cdot V_i}{\sqrt{3} \cdot 2\pi \cdot f \cdot L} \right)$  parameter of the converter, using the critical inductance  $L$  given by Eq. (6).

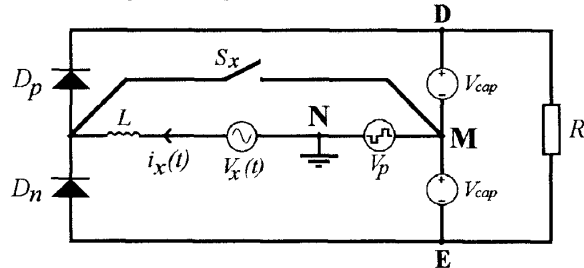


Figure 5: Simplified equivalent circuit for the circuit analysis. The diodes and the bi-directional switch are supposed with ideal characteristics.  $L$  is the "critical inductance" of the converter.

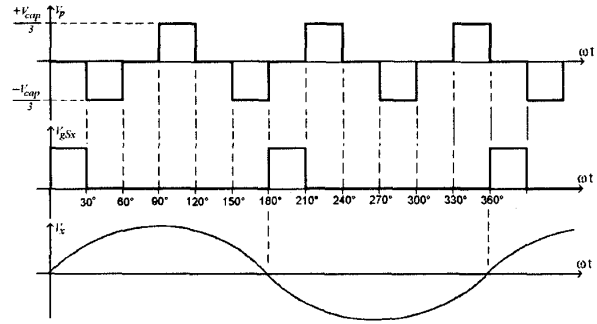


Figure 6: Voltage pattern of the  $V_p$  pulsed source and the  $V_x$  sinusoidal source, along with the switching pattern for the  $S_x$  switch, of the simplified equivalent circuit shown in Fig. 5.

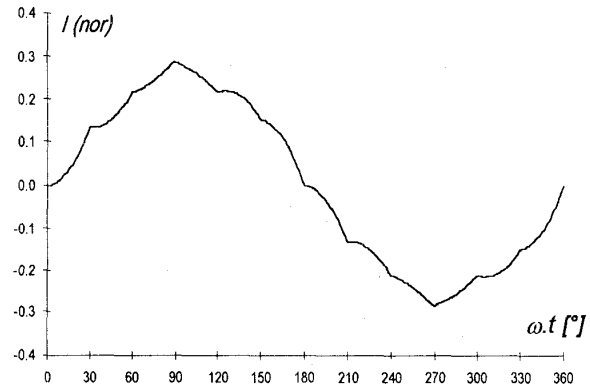


Figure 7: Computer-generated plot of the input current of the AC to DC converter for one cycle of the input voltage, obtained with the equations shown in Table 1.

With the Fourier analysis of the generalized waveform shown in Fig. 7, the theoretical value of the Total Harmonic Distortion (THD) of the input current is 6.07 % and the Power Factor of the converter is expected to be greater than 0.99. Also with the set of equations in Table 1, the collection of expressions for the maximum current values through any of the elements is effortless. For instance, it can be noticed in Fig. 4 that during the  $0^\circ - 30^\circ$  stage the input current  $i_a$  flows totally through the bi-directional switch. As result, the maximum current through each switch is given by Eq. (7):

$$I_{sw(max)} = \frac{V_i}{f \cdot L} \left[ 1 - \frac{\sqrt{3}}{2} \right] \frac{\sqrt{2}}{2\pi\sqrt{3}} = 1.741 \times 10^{-2} \left( \frac{V_i}{f \cdot L} \right) \quad (7)$$

The maximum voltage across each bi-directional switch, as seen in Fig. 4, is  $\frac{1}{2}$  of the output voltage, or:

$$V_{sw(max)} = \frac{13366 \cdot V_i}{2} = 0.6683 \cdot V_i \quad (8)$$

On the other hand, from Eq. (6) a expression for the output power can be obtained:

$$P_o = 38489 \times 10^{-2} \cdot \frac{(V_i)^2}{f \cdot L} \quad (9)$$

Table 1: Equations for the input current on each stage, derived from the analysis of the equivalent simplified circuit.  
For the 180° to 360° period, the same equations can be used, multiplied by (-1).

Stage	Equation for the input current	Current at the end of the stage
0 to 30°	$\frac{V_i}{f \cdot L} [1 - \cos(\omega \cdot t)] \frac{\sqrt{2}}{2\pi\sqrt{3}}$	$\frac{V_i}{f \cdot L} \left[1 - \frac{\sqrt{3}}{2}\right] \frac{\sqrt{2}}{2\pi\sqrt{3}}$
30° to 60°	$\frac{V_i}{f \cdot L} \left[\frac{9}{7} - \cos(\omega \cdot t) - \frac{12}{7 \cdot \pi} (\omega \cdot t)\right] \frac{\sqrt{2}}{2\pi\sqrt{3}}$	$\frac{V_i}{f \cdot L} \left[\frac{3}{14}\right] \frac{\sqrt{2}}{2\pi\sqrt{3}}$
60° to 90°	$\frac{V_i}{f \cdot L} \left[\frac{11}{7} - \cos(\omega \cdot t) - \frac{18}{7 \cdot \pi} (\omega \cdot t)\right] \frac{\sqrt{2}}{2\pi\sqrt{3}}$	$\frac{V_i}{f \cdot L} \left[\frac{2}{7}\right] \frac{\sqrt{2}}{2\pi\sqrt{3}}$
90° to 120°	$\frac{V_i}{f \cdot L} \left[2 - \cos(\omega \cdot t) - \frac{24}{7 \cdot \pi} (\omega \cdot t)\right] \frac{\sqrt{2}}{2\pi\sqrt{3}}$	$\frac{V_i}{f \cdot L} \left[\frac{3}{14}\right] \frac{\sqrt{2}}{2\pi\sqrt{3}}$
120° to 150°	$\frac{V_i}{f \cdot L} \left[\frac{10}{7} - \cos(\omega \cdot t) - \frac{18}{7 \cdot \pi} (\omega \cdot t)\right] \frac{\sqrt{2}}{2\pi\sqrt{3}}$	$\frac{V_i}{f \cdot L} \left[\frac{\sqrt{3}}{2} - \frac{5}{7}\right] \frac{\sqrt{2}}{2\pi\sqrt{3}}$
150° to 180°	$\frac{V_i}{f \cdot L} \left[\frac{5}{7} - \cos(\omega \cdot t) - \frac{12}{7 \cdot \pi} (\omega \cdot t)\right] \frac{\sqrt{2}}{2\pi\sqrt{3}}$	zero

As there are three active switches in the converter ( $S_a$ ,  $S_b$  and  $S_c$ ), the “power ratio of the active switches” is given by Eq. (10):

$$\psi = \frac{3 \cdot (I_{sw(max)} \cdot V_{sw(max)})}{P_o} \quad (10)$$

Using Equations (7), (8) and (9) in Eq. (10),  $\psi = 0.907$  is obtained.

### III. THE 7.4 kW PROTOTYPE

The first laboratory prototype was assembled to validate the proposed converter and the circuit analysis, with power circuit as shown in Fig. 2. The main characteristics of the first prototype were:

- Input phase-to-phase AC voltage: 220 V, 60 Hz.
- DC Output Power: 7.4 kW

The “critical inductance” is calculated with Eq. (6):

$$L = 3.8489 \times 10^{-2} \cdot \frac{(V_i)^2}{f \cdot P_o} = 3.8489 \times 10^{-2} \cdot \frac{(220)^2}{60 \times 7400} = 4.19 \text{ mH}$$

The DC output voltage for the nominal power output is calculated with Eq. (5):

$$V_o = 1.3366 \cdot V_i = 1.3366 \times 220 = 294.1 \text{ V}$$

The circuit was then simulated using PSpice. Figure 8 shows the input current through one of the input inductors with the corresponding input phase voltage. It can be noticed that the simulated current waveform is similar to the one obtained with the theoretical analysis and displayed in Fig. 7. The PSpice Fourier analysis gives a THD of 6.3 % for the input current, resulting to a Power Factor of 0.998.

As a result, the first prototype was build with three 4 mH silicon-steel core inductors for  $L_a$ ,  $L_b$  and  $L_c$ . Each inductor weights about 2.9 kg (6.4 lb).

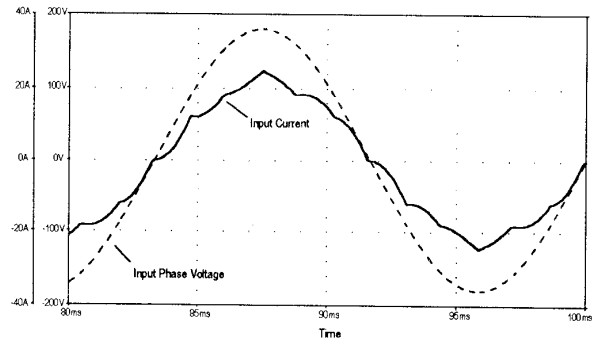


Figure 8: PSpice circuit simulation of the input current and corresponding input phase voltage.

The bi-directional switches  $S_a$ ,  $S_b$  and  $S_c$  were assembled with IRF740 Power MOSFETs connected between the DC nodes of rectifier bridges, as in Fig. 9. For diodes  $D_a$ ,  $D_b$ ,  $D_c$  and  $D_d$ , Semikron SK3G/04 were used.

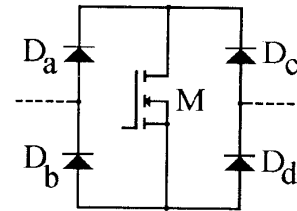


Figure 9: Assembly for each bi-directional switch  $S_a$ ,  $S_b$  and  $S_c$  used in the prototypes.

An elementary circuit was used to generate the gate pulses for the MOSFETs, with gate widths of 1.39 ms, equivalent to 30° on a 60 Hz system. For  $C_a$  and  $C_b$ , 1000  $\mu\text{F}$  electrolytic capacitors were used.

Bench tests of the first prototype were conducted with an assortment of high-power wire resistors connected to the output of the prototype. Figure 10 shows the waveforms of the input current and the corresponding phase voltage, for 7.45 kW output power. At that load condition, the measured output voltage was 291.5 V. The Fourier analysis of the input current shown in Fig. 10 results in a Total Harmonic Distortion (THD) of 6.6 % and the corresponding power factor is 0.996.

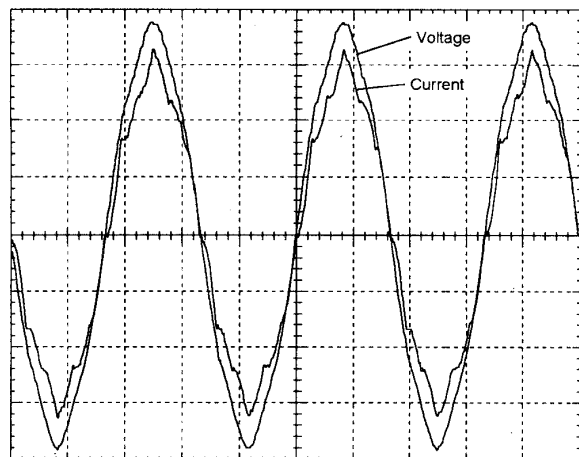


Figure 10: Experimental Input Current and Phase Voltage for the first prototype at 7.45 kW output power. Scales: Voltage = 50 V/div.; Current = 10 A/div.; Time = 5 ms/div.

#### IV. THE 12 kW PROTOTYPE

As the foremost result of the theoretical analysis, the equations shown in Table 1 entitle the calculation of the current through every element of the proposed circuit, along with the voltage stresses on the switches. To simplify the design of converters employing the proposed topology, a computer program was developed to perform the calculation process. The computer program asks the user to enter the phase-to-phase AC input voltage, the AC frequency and the desired DC output power. An output report is thereafter generated, with the calculated current values for the power switches and diodes and voltage stresses. With this report the user can easily choose in commercial data books the semiconductor components for the converter assembly and design the input inductors.

By way of illustration, a second prototype was proposed, with its main characteristics:

- Input phase-to-phase AC voltage: 220 V, 60 Hz.
- DC Output Power: 12 kW

Table 2 lists the design data obtained with the computer program.

For the main rectifier, Semikron SKR26/04 diodes (cathode stud) were used for  $D_1$ ,  $D_2$  and  $D_3$ , along with SKN26/04 diodes (anode stud) for  $D_4$ ,  $D_5$  and  $D_6$ . For the bi-directional switches' assembly (Fig. 9), APT6040BN power MOSFETs were used, in addition to four Semikron SK3G10 diodes for each switch.

Table 2: Output data of the computer program for the design of the 12 kW prototype.

AC Input	phase-to-phase voltage AC frequency	220 V 60 Hz
DC Output	output power output voltage for nominal load average current for nominal load	12000 W 294.05 V 40.81 A
Input Inductors	critical inductance maximum current rms current	2.58 mH 52.36 A 34.02 A
Bi-Directional Switches	switch maximum current switch rms current switch average current switch "off" voltage diode maximum current diode rms current diode average current diode reverse voltage	24.55 A 4.51 A 1.38 A 147.03 V 24.55 A 3.19 A 0.69 A 147.03 V
Rectifier Diodes	rms current average current reverse voltage	23.84 A 14.58 A 294.05 V
Load Capacitors	rms current DC voltage	2.26 A 147.03 V

The input inductors were constructed with silicon-steel sheet cores, with 2.6 mH inductance. Each inductor weights 3.5 kg (7.7 lb) and has an air gap for fine inductance adjustment at the laboratory. The gate circuit is the same from the first prototype.

In the same way as the first prototype, bench tests were conducted with the 12 kW prototype using several high-power resistors connected as the load. The maximum output power achieved was 11.94 kW, with output voltage of 296.1 V. Figure 11 shows the input current and input phase voltage for that load condition. The Fourier analysis on the current trace from Fig. 11 results in THD = 10.5 % and thereafter a Power Factor of 0.994 is accomplished.

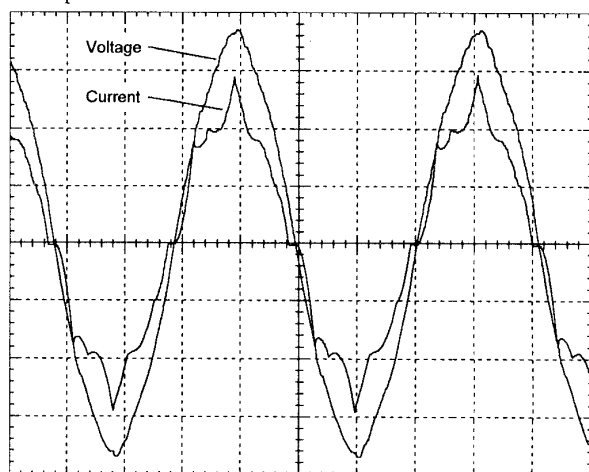


Figure 11: Experimental Input Current and Phase Voltage for the second prototype at 11.94 kW output power. Scales: Voltage = 50 V/div.; Current = 20 A/div.; Time = 4 ms/div.

Figure 12 shows the behavior of the 12 kW prototype for variable load condition and three different values of the gate pulse width ( $\alpha$ ). It can be noticed in Fig. 12 that at light load condition the output voltage is increased and also that the gate pulse width can be used as a control variable for the output voltage regulation. The use of the low-frequency gate pulse width for voltage regulation was presented in detail in [2] and [4] and therefore is not covered in the present work.

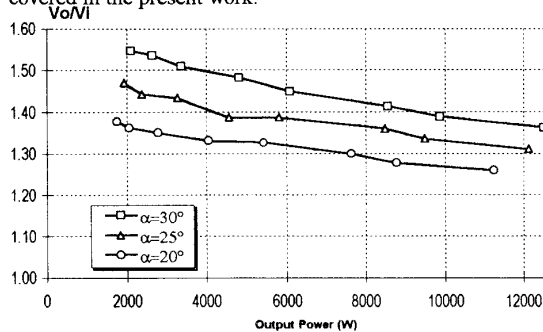


Figure 12: Output characteristic of the 12 kW prototype.

Daniel, Chaffai and Al-Haddad [5] have also reported the possibility of a novel control technique in the proposed converter. In that proposal, each bi-directional switch  $S_a$ ,  $S_b$  and  $S_c$  can be gated using width-modulated pulses (PWM) during a  $60^\circ$  interval ( $30^\circ$  before the zero-volt transition and  $30^\circ$  after the transition), achieving good output voltage regulation and low distortion level over an extended power output range.

## V. CONCLUSIONS

This paper presents the analysis of a three-phase diode rectifier with three low-frequency auxiliary switches, that can achieve a high power factor with a simple switching technique. With the introduction of the "critical inductance" of the rectifier, the analysis showed that the converter can be modeled by an elementary equivalent circuit, from where a set of linear equations was obtained. The DC output voltage is thereafter calculated, along with the "critical inductance" as a function of the rated DC output power. With the equivalent circuit it was also possible to calculate

the generalized input current waveform, showing that the power factor of the proposed circuit is over 0.99, with theoretical THD of the input current under 6.1%, for nominal load.

Two laboratory prototypes with 7.4 kW and 12 kW output power were build and evaluated through bench tests. The results showed that the analysis technique can be used to design high power rectifiers with low-cost input inductors, achieving high power factor and low figures of THD on the input current. Using the equations obtained from the circuit analysis, an elementary computer program was developed to calculate all the design parameters of converters making use of the proposed circuit.

The computer program mentioned in this work runs under Microsoft Windows® and can be obtained by writing to the first author or downloaded through the Internet from:

<http://www.eletr.ufpr.br/users/mehl/psc96.html>

## REFERENCES

- [1] A. R. Prasad, P. D. Ziogas and S. Manias, "An active power factor correction technique for three-phase diode rectifiers" *IEEE Power Electronics Specialists Conference (PESC'89) Records*, pp. 58-66, June 1989.
- [2] E. L. M. Mehl and I. Barbi, "An Improved High Power Factor and Low Cost Three-Phase Rectifier". *IEEE Applied Power Electronics Conference (APEC'95) Proceedings*, pp. 835-841, March 1995.
- [3] J. W. Kolar and F. C. Zach, "A novel three-phase three-switch three-level unity power factor PWM rectifier", *28th PCIM Conference (Nürnberg, Germany)*, June 1994.
- [4] E. L. M. Mehl. "Proposition, Analysis, Design and Practical Implementation of a New Three-Phase Rectifier with High Power Factor" Doctorate Thesis, Universidade Federal de Santa Catarina, Brazil, 1996. (in Portuguese)
- [5] F. Daniel, R. Chaffai and K. Al-Haddad. "Three-Phase Diode Rectifier with Low Harmonic Distortion to Feed Capacitive Loads". *IEEE Applied Power Electronics Conference (APEC'96) Proceedings*, pp. 932-938, March 1996.